Supplementary Information for

Enhancing Electromechanical Responsiveness of PVC Gels via Ion Size Control

Kazuki Takahashi, Osamu Urakawa, Tadashi Inoue

Department of Macromolecular Science, Graduate School of Science, Osaka University
1-1 Machikaneyama-cho, Toyonaka, Osaka 560-0043, Japan.

Contents:

S1. Dielectric Relaxation Behavior of PVC/DBA/EMIM-TFSI Gels

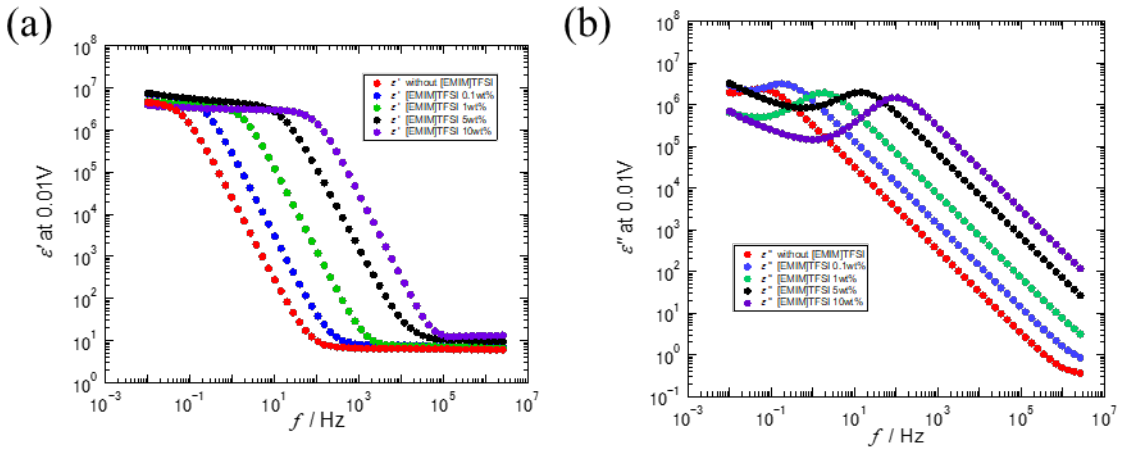

Figure S1. Frequency dependence of dielectric constant ε' (a) and dielectric loss ε'' (b) for PVC/DBA/EMIM-TFSI gels with various salt concentrations.

S2. Nonlinear Dielectric Relaxation Behaviors for PVC/DBA and PVC/DBA/EMIM-TFSI Gels

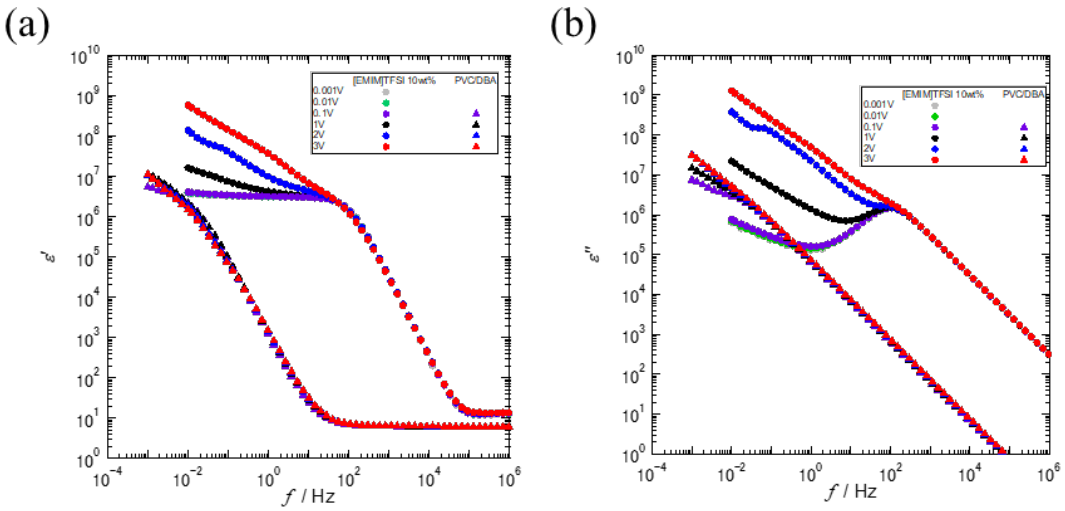

Figure S2. Applied voltage dependence of ε' and ε'' for PVC/DBA and PVC/DBA/EMIM-TFSI (PVC: DBA = 1:6, $n = 5.35 \times 10^{-5}$ mol g^{-1}) gel systems.

S3. Details of the Current Absorption Method

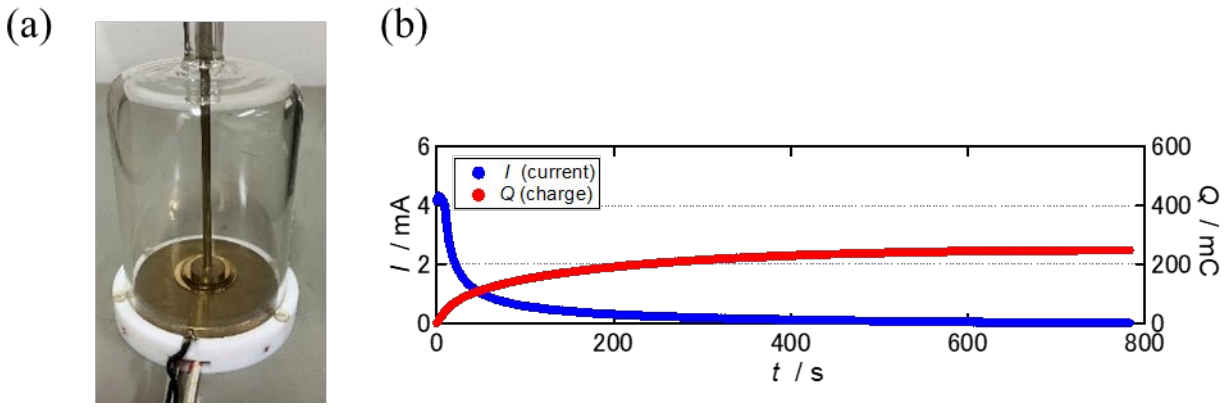

Figure S3. (a) The electrode cell used for the current absorption method (b) Measured current and calculated charge $Q(t) = \int_0^t I(\tau)d\tau$.

The complex permittivity under high-voltage conditions was calculated from the $Q(t)$ data shown in Figure S3(b) using Equations (2) and (3).

S4. Temperature Rise Due to Joule Heating and the Resulting Change in Elastic Modulus

We examine whether the enhanced bending induced by the addition of ionic liquids can be explained by Joule heating caused by the increased current and the resulting thermal softening.

S4-1 Formulation of Temperature Rise Calculation Based on Measured Current Values

Figure S4 shows the time-dependent current, $I(t)$, flowing through the gel sample during the deformation experiment under an applied voltage, which was measured simultaneously to evaluate the electrical energy input.

Because the applied voltage V remained nearly constant during the measurement, the instantaneous heat generation rate, $P_{in}(t)$, is given by

$$P_{in}(t) = VI(t) \quad \text{(S1)}$$

Accordingly, the electrical energy input into the sample up to time t, $Q_{in}(t)$, is expressed as

$$q_{in}(t) = \int_0^t P_{in}(\tau)d\tau \quad \text{(S2)}$$

The heat generated in the gel was assumed to diffuse primarily toward the SUS electrodes on both sides. The thermal resistance between the gel and the SUS electrodes, R_{th}, was approximated using the thermal conductivity of the gel, λ_{gel}, as follows. (Because the thermal conductivity of SUS is much higher than that of the gel, the thermal resistance is assumed to be dominated by the gel.)

$$R_{th} = \frac{d/2}{\lambda_{gel}A} \quad \text{(S3)}$$

Here, $d$is the gel thickness between the electrodes, and $A$is the contact area of the gel with the electrodes (including both sides). The heat flow, $P_{\mathrm{dis}}(t_k)$, diffusing from the gel to the SUS electrodes at time t_k, can be written as follows.

$$P_{dis}(t) = \left[T_{gel}(t) - T_{sus}(t)\right]/R_{th} \tag{S4}$$

Therefore, the time evolution of the gel temperature and the SUS electrode temperature can be calculated sequentially using the following equations based on the heat balance.

$$T_{gel}(t + \Delta t) = T_{gel}(t) + \frac{[P_{in}(t) - P_{dis}(t)]\Delta t}{C_{gel}m_{gel}} \tag{S5}$$

$$T_{SUS}(t + \Delta t) = T_{SUS}(t) + \frac{P_{dis}(t)\Delta t}{C_{sus}m_{sus}} \tag{S6}$$

Here, C_{gel}, C_{sus}, m_{gel}, and $m_{\mathrm{sus}}$are the specific heats at constant pressure and masses of the gel and SUS electrodes, respectively. The value of $C_{\mathrm{gel}}$was estimated as the weighted average of the specific heats of PVC and DBA based on their weight fractions.

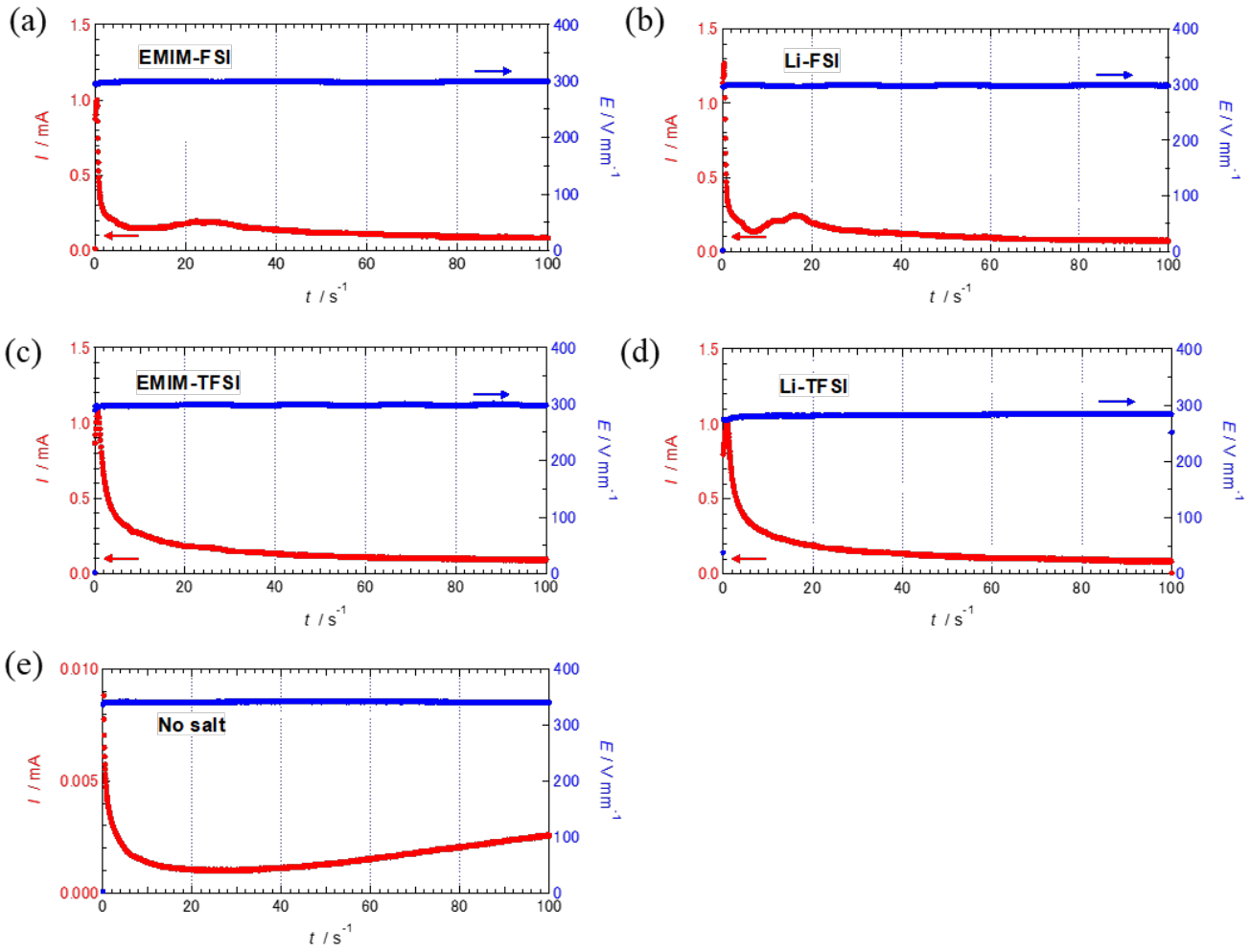

Figure S4. Measured time-dependent voltage $V(t)$ and current $I(t)$, for the (a)EMIM-FSI, (b)EMIM-TFSI, (c)Li-FSI, (d)Li-TFSI, and (e)no salt gels.

S4-2 Physical Properties and Geometrical Parameters Used in the Calculation

To evaluate the temperature rise of the gel sample and the electrodes using Equations (S5) and (S6), the parameters listed in Table S1 were employed. To avoid underestimating the temperature rise, all physical parameters were conservatively chosen to favor larger temperature increases, corresponding to conditions in which heat diffusion is less efficient. The dimensions, densities, specific heats, and thermal conductivities of the gel and SUS electrodes were determined based on experimentally measured values.

The thermal conductivity of the gel, λ_{gel}, was assumed to be 0.13 W m^{-1} K^{-1}. This value was chosen conservatively from the reported thermal conductivities of PVC (0.16 W m^{-1} K^{-1}) and DBA (0.13–0.15 W m^{-1} K^{-1}), specifically selecting the lower value corresponding to less efficient heat dissipation.

Table S1. Physical parameters used for the thermal simulation.

Symbol	Value	Description
$T_{gel,0}, T_{SUS,0}$	25℃	Initial temperature
Δt	0.05 s	Sampling interval of the data logger
$C_{,PVC}$	1.04×10^3 J kg^{-1} K^{-1}	Specific heat of PVC, literature value *1
C_{DBA}	1.92×10^3 J kg^{-1} K^{-1}	Specific heat of DBA, literature value *3
$C_{,gel}$	1.79×10^3 J $kg^{-1}K^{-1}$	Specific heat of the gel, calculated value
C_{SUS}	5×10^2 J $kg^{-1}K^{-1}$	Specific heat of SUS, literature value *4
λ_{gel}	0.13 W $m^{-1}K^{-1}$	Thermal conductivity of the gel, literature values *2,*3
λ_{SUS}	15 W $m^{-1}K^{-1}$	Thermal conductivity of SUS, literature value *4
d_{gel}	1×10^{-3} m	Gel thickness, experimentally measured value
A	4.0×10^{-5} m	Contact area between the gel and electrodes
m_{gel}	2.04×10^{-5} kg	Calculated from density × volume
m_{SUS}	3.95×10^{-3} kg	Calculated from density × volume
R_{th}	96.2 K W^{-1}	Thermal resistance

Notes for Table S1:

*1 Specific heat of PVC: Chang, S.-S. *Heat capacity and thermodynamic properties of poly(vinyl chloride). J. Res. Natl. Bur. Stand.* **1977**, *82*, 9–18.
*2 Thermal conductivity of PVC: Ebadi-Dehaghani, H.; Nazempour, M. *Thermal Conductivity of Nanoparticles Filled Polymers.* In *Smart Nanoparticles Technology*; Hashim, A. A., Ed.; IntechOpen, 2012.
*3 Specific heat and thermal conductivity of DBA: estimated from the thermophysical property database "WTT (ThermoData Engine)" provided by the National Institute of Standards and Technology (NIST).
*4 Density, specific heat, and thermal conductivity of SUS: Japan Stainless Steel Association (JSSA), "Comparison with Other Materials", available at:
JSSA Comparison with Other Materials
(accessed April 17, 2026).

S4-3. Calculation Results

Figure S5 shows the simulation results. As seen in this figure, the gel temperature increased immediately after the onset of current flow and subsequently approached saturation due to the balance between heat generation and thermal diffusion. The maximum temperature observed for the EMIM-TFSI gel was $T_{\max} = 37.4$℃, corresponding to a temperature rise of $\Delta T_{\max} = 12.4$℃ from the initial temperature, $T_{\mathrm{gel},0} = T_{\mathrm{SUS},0} = 25$℃.

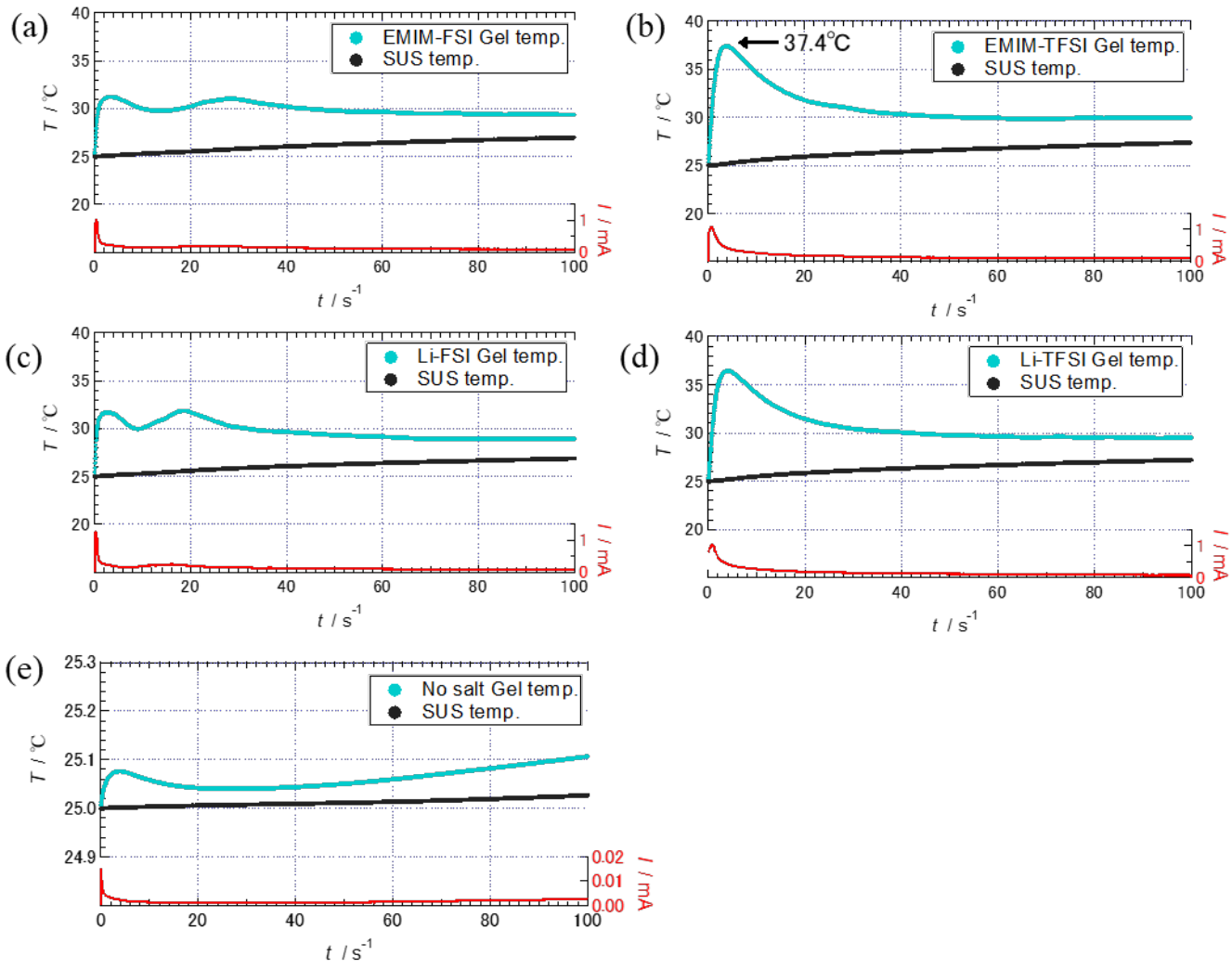

Figure S5. Simulated temperature evolution of the (a)EMIM-FSI, (b)EMIM-TFSI, (c)Li-FSI, (d)Li-TFSI and (e)no salt gel and SUS electrode.

Importantly, this value represents an upper-bound estimate obtained using physical parameters selected to maximize the temperature rise. Therefore, the actual sample temperature is likely lower than the value estimated here. Furthermore, because heat dissipation to the surrounding air was not explicitly included in the model, the temperature rise is expected to be overestimated relative to the actual experimental conditions.

S4-4. Effect of temperature rise on the elastic modulus of the gel

Next, the effect of the maximum temperature, $T_{\max} = 37.4$ ℃, on the elastic modulus of the gel was examined. Figure S6 shows the temperature dependence of the storage modulus, G', of the gel measured using a parallel plate geometry at γ=5% over the temperature range from 20 to 80 ℃. The modulus at $T_{\max}$ was lower than that at room temperature (25 ℃), but instead increased slightly, indicating that the observed enhancement in bending cannot be attributed to thermal softening caused by Joule heating.

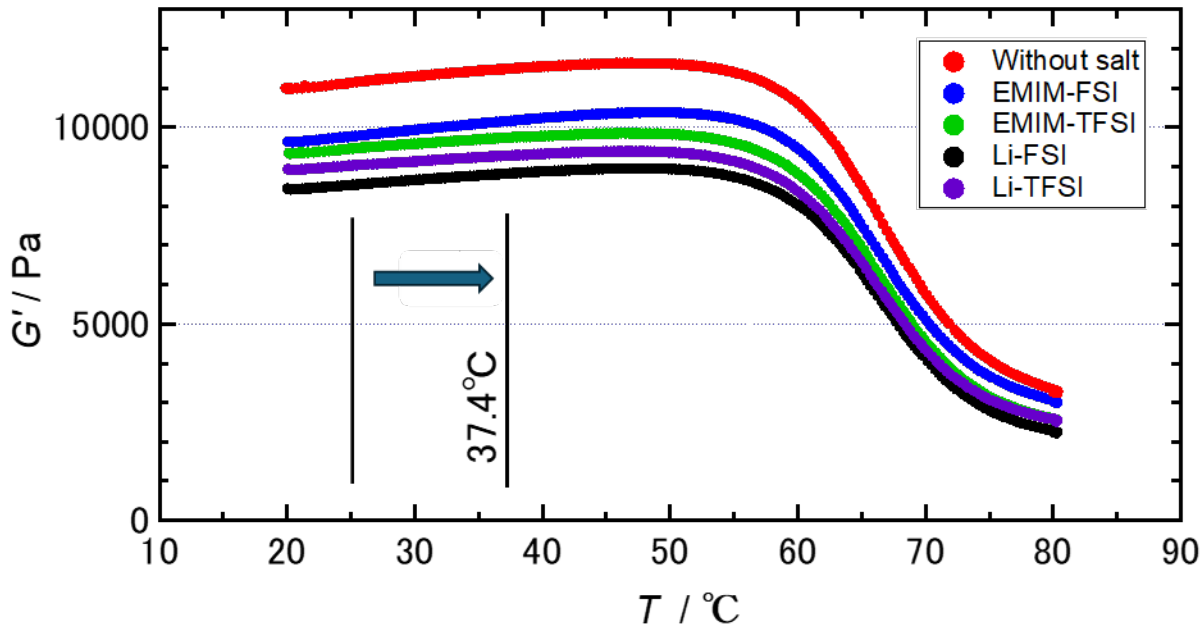

Figure S6. Temperature dependence of storage modulus.

S5. Numerical Data for the Electric-Field Response Tests

Tabel S2. Sample thickness in dielectric measurements within (a) the low voltage (0.001V~3V) region, (b) the high voltage (170V) region

	PVC/DBA	EMIMFSI	EMIMTFSI	LiFSI	LiTFSI
(a) Sample thickness / mm	1.63	1.25	1.19	1.24	1.35
(a) Sample thickness / mm	1.44	1.44	1.34	1.54	1.39

Table S3. $\boldsymbol{\theta_\infty}$ and $\boldsymbol{\tau_\theta}$ for PVC/DBA gel and all PVC/DBA/salt gels after applying a constant electric field of 300 V mm^{-1} for 100 seconds.

	PVC/DBA	EMIMFSI	EMIMTFSI	LiFSI	LiTFSI
$\theta_\infty / °$	5.18	99.20	50.0	79.9	35.2
τ_θ / s	16.8	43.4	44.7	56.0	32.9

S6. Cyclic Deformation Tests

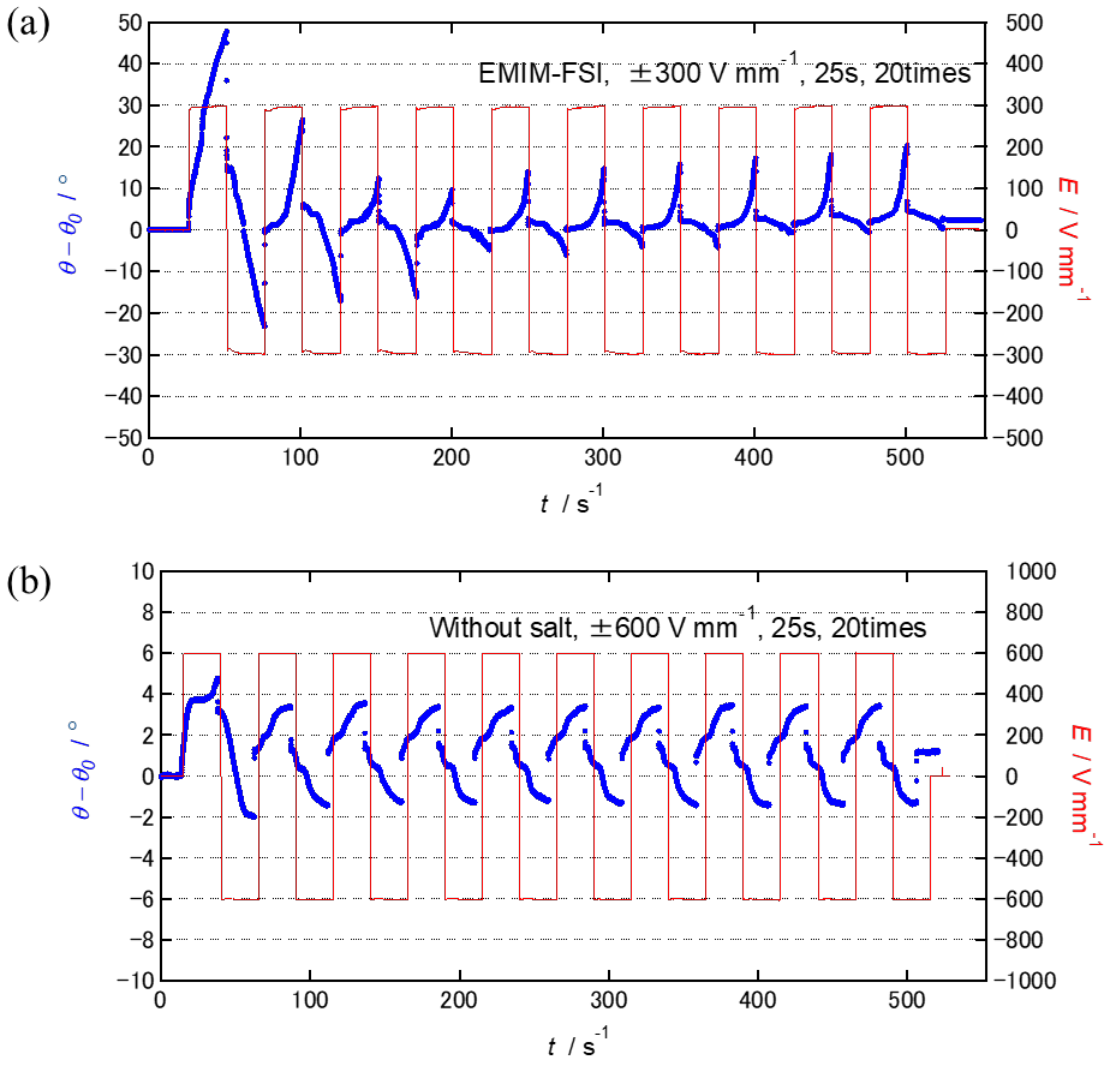

Figure S7. Time dependence of the bending angle (blue symbols) for the EMIM-FSI-containing system (a) and the salt-free system (b) under repeated reversal of the pulsed voltage (red line in the figure).

S7. Thickness Dependence of the Bending Behavior

Figure S8 compares the bending behavior of EMIM-FSI-containing gels with different thicknesses under the same electric field strength (300 Vmm^{-1}). If the actuation behavior were governed solely by the ion migration distance, thinner gels would be expected to exhibit faster and larger deformation because of the shorter migration path and lower bending rigidity, respectively. However, the experimental results showed no systematic dependence on thickness: during the initial stage of electric field application, larger bending deformation was observed for thicker gels, while the deformation time scales remained comparable. This tendency is particularly noteworthy because the bending rigidity generally increases with the cube of the thickness.

In addition, the thickest gel (2 mm, 600 V) exhibited a non-monotonic transient response, where the bending angle partially relaxed after the initial deformation. This behavior suggests the presence of additional nonlinear interfacial effects under high-voltage conditions. These results imply that the bending mechanism is more complex than a simple bulk ion migration process and may involve local electric-field concentration and interfacial phenomena near the electrode edge.

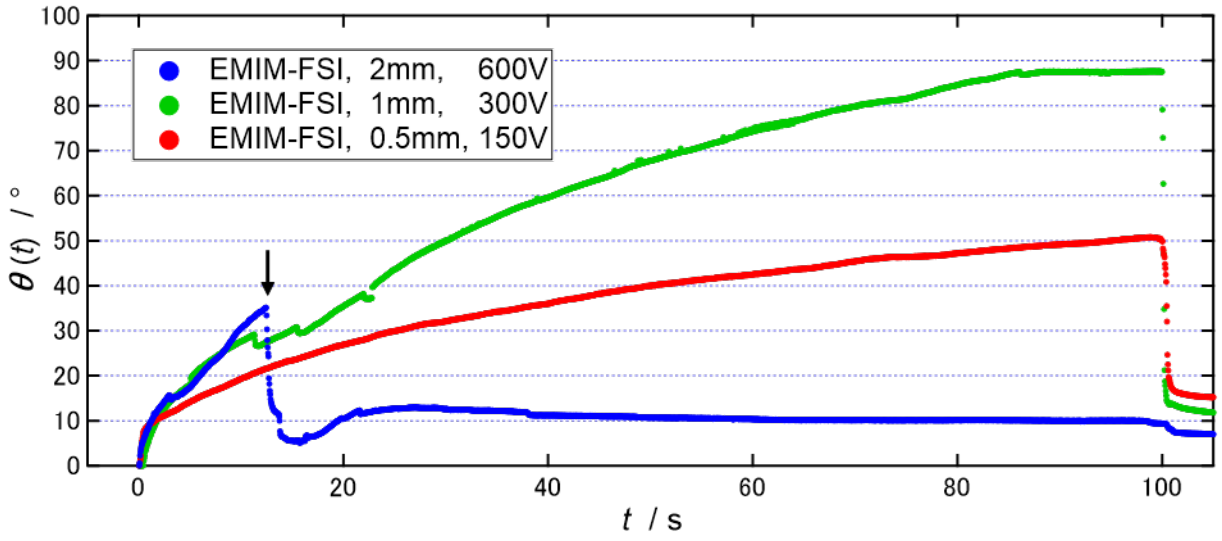

Figure S8. Time dependence of the bending angle, $\theta(t)$, for EMIM-FSI-containing gel actuators with different gel thicknesses (0.5, 1.0, and 2.0 mm) measured under the same electric field strength (300 V mm^{-1}). The applied voltages were adjusted according to the gel thickness (150, 300, and 600 V for 0.5, 1.0, and 2.0 mm, respectively). The thickest gel (2.0 mm) exhibited a non-monotonic transient response, in which the bending angle partially relaxed after the initial deformation.